nescence is visible to the naked eye, although it is noticeably less intense and shifted to higher energy with respect to the emission spectrum of the parent (non–polymer-containing) Si dispersion in toluene. This shift is attributed to oxidation of the Si particles during the casting process. Similar shifts in the emission spectra have been observed upon exposure of porous Si to air (*32*). The pure toluene and polystyrene films showed no detectable luminescence.

Transmission electron microscope (TEM) images were obtained by pipetting a drop of the Si colloidal suspension onto the middle of a polystyrene-dipped TEM grid (Cu mesh) in air. In the microscopy we used a Philips CM30 TEM at an acceleration voltage of 100 or 300 keV. Si particles attached to thin regions and near holes in the polystyrene could be studied (Fig. 3). Crystalline, overlapping Si particles are clearly visible against an amorphous polystyrene background. The particles are irregularly shaped and range in size from many micrometers down to the resolution limit of the TEM (about 0.2 nm). This image is consistent with the known structural properties of bulk porous Si as seen from TEM and scanning electron microscopy (*33–35*). The inset shows a selected area diffraction pattern clearly identifiable as polycrystalline Si. The edges of each particle and the smallest particles are very thin, less than 10 nm thick. Convergent beam diffraction showed these regions to be predominantly amorphous, although TEM images of luminescent porous Si have recently been reported showing small crystalline regions (*36*). The lack of crystallinity observed in the present work is possibly the result of oxidation during exposure to air or electron beam damage during microscopy. Presumably the smaller particles and the thin regions on the larger particles are responsible for the luminescence observed in these samples, as quantum confinement effects are expected to appear in Si particles no larger than several nanometers (*1–3*).

REFERENCES AND NOTES

1. A. Henglein, *J. Chim. Phys. Physicochim. Biol.* **84**, 1043 (1987).
2. ______, *Chem. Rev.* **89**, 1861 (1989).
3. L. Brus, *J. Phys. Chem.* **90**, 2555 (1986).
4. A. Fojtik, H. Weller, S. Fiechter, A. Henglein, *Chem. Phys. Lett.* **134**, 477 (1987).
5. H. Takagi, H. Ogawa, Y. Yamazaki, A. Ishizaki, T. Nakagiri, *Appl. Phys. Lett.* **56**, 2379 (1990).
6. C. J. Sandroff *et al.*, *Science* **245**, 391 (1989).
7. M. A. Olshavsky, A. N. Goldstein, A. P. Alivisatos, *J. Am. Chem. Soc.* **112**, 9438 (1990).
8. Y. Wang, *Acc. Chem. Res.* **24**, 133 (1991).
9. R. Jain and R. Lind, *J. Opt. Soc. Am.* **75**, 647 (1983).
10. R. A. Morgan, S.-H. Park, S. W. Koch, N. Peyghambarian, *Semicond. Sci. Technol.* **5**, 544 (1990).
11. Y. Wang, A. Suna, W. Mahler, R. Kasowski, *J. Chem. Phys.* **87**, 7315 (1987).
12. T. Rajh, M. I. Vucemilovic, N. M. Dimitrijevic, O. I. Micic, A. J. Nozik, *Chem. Phys. Lett.* **143**, 305 (1988).
13. Y. Wang and N. Herron, *J. Phys. Chem.* **91**, 257 (1987).
14. T. Dannhauser, M. O'Neil, K. Johansson, D. Whitten, G. McLendon, *ibid.* **90**, 6074 (1986).
15. C.-H. Fischer and A. Henglein, *ibid.* **93**, 5578 (1989).
16. S. Gallardo, M. Gutierrez, A. Henglein, E. Janata, *Ber. Bunsenges. Phys. Chem.* **93**, 1080 (1989).
17. M. Haase, H. Weller, A. Henglein, *J. Phys. Chem.* **92**, 482 (1988).
18. D. Hayes, O. I. Micic, M. T. Nenadovic, V. Swayambunathan, D. Meisel, *ibid.* **93**, 4603 (1989).
19. P. V. Kamat, T. W. Ebbesen, N. M. Dimitrijevic, *Chem. Phys. Lett.* **157**, 384 (1989).
20. D. Meisel and W. A. Mulac, *Coll. Surf.* **35**, 179 (1989).
21. M. O'Neil and G. McLendon, *Chem. Phys. Lett.* **147**, 565 (1988).
22. L. Spanhel, M. Haase, H. Weller, A. Henglein, *J. Am. Chem. Soc.* **109**, 5649 (1987).
23. Y. Wang and N. Herron, *J. Phys. Chem.* **91**, 5005 (1987).
24. D. J. DiMaria *et al.*, *J. Appl. Phys.* **56**, 401 (1984).
25. V. Lehmann and U. Gosele, *Appl. Phys. Lett.* **58**, 856 (1990).
26. L. T. Canham, *ibid.* **57**, 1046 (1990).
27. A. Halimaoui *et al.*, *ibid.* **59**, 304 (1991).
28. T. Ito, H. Kiyama, T. Yasumatsu, H. Watabe, A. Hiraki, *Physica B* **170**, 535 (1991).
29. P. Gupta, V. L. Colvin, S. M. George, *Phys. Rev. B* **37**, 8234 (1988).
30. N. S. Lewis, *J. Electrochem. Soc.* **131**, 2496 (1984).
31. D. F. Shriver and M. A. Drezdzon, *The Manipulation of Air-Sensitive Compounds* (Wiley, New York, 1986).
32. L. T. Canham, M. R. Houlton, W. Y. Leong, C. Pickering, J. M. Keen, *J. Appl. Phys.* **70**, 422 (1991).
33. M. D. Drory, P. C. Searson, L. Liu, *J. Mater. Sci. Lett.* **10**, 81 (1991).
34. S. F. Chuang, S. D. Collins, R. L. Smith, *Appl. Phys. Lett.* **55**, 1540 (1989).
35. G. Bomchil and A. Halimaoui, *Appl. Surf. Sci.* **41/42**, 604 (1989).
36. A. G. Cullis and L. T. Canham, *Nature* **353**, 335 (1991).
37. The work of G.M.C. was supported by the NSF Young Scholars Program.

9 September 1991; accepted 5 November 1991

Strontium Isotopic Composition of Estuarine Sediments as Paleosalinity-Paleoclimate Indicator

B. L. INGRAM AND D. SLOAN

The strontium isotopic composition of biogenic precipitates that occur in estuarine sediments can be used as proxy indicator of paleosalinity and for assessing precipitation and river discharge rates over thousands of years. In the San Francisco Bay estuary, river water with low $^{87}Sr/^{86}Sr$ ratio (average, 0.7065) and low Sr concentration (0.13 parts per million) mixes with seawater with a higher $^{87}Sr/^{86}Sr$ ratio (0.7092) and Sr concentration (7.9 parts per million). The predicted mixing relation between salinity and Sr isotopic composition is confirmed by measurements of modern estuarine surface waters. A paleosalinity record obtained from foraminifera for the ancestral San Francisco Bay during oxygen isotope substage 5e of the last interglacial reflects a global rise and fall of sea level, and short time-scale variations related to fluctuations in discharge rates of the Sacramento and San Joaquin rivers.

ESTUARIES ARE GEOLOGICALLY short-lived features, existing mainly during times of relatively high sea level; but, because estuaries are sensitive to climatic changes, the geochemistry and faunal assemblages in estuarine sediments are an important source of paleoclimatic and paleohydrologic information. In this paper, we describe a geochemical method of determining paleosalinity of estuarine waters and report results obtained from San Francisco Bay, the largest estuarine system on the west coast of North America, for oxygen isotope substage 5e of the last interglacial (about 120,000 years before present). As San Francisco Bay receives freshwater from 40% of the surface area of California (162,000 km^2) by way of the Sacramento and San Joaquin rivers and their tributaries (Fig. 1) (*1*), salinity variations in the geologic record provide a proxy for precipitation and runoff from a large continental area. Because streamflow in the western United States and Hawaii reflects large-scale North Pacific winter atmospheric circulation, the Sr isotopic data may have broad paleoclimatic and paleohydrologic implications (*2*).

The salinity of San Francisco Bay water is a function of freshwater inflow rates and sea level; the latter controls the entry of saline (33 to 35 per mil) ocean water into the bay through the Golden Gate (Fig. 2) (*1, 3*). The inflow of freshwater is seasonal; maximum river discharge occurs during winter and early summer, reflecting winter rains and spring snowmelt (*1*). Because most of the state's annual precipitation falls in northern California, 80% of the freshwater enter-

---

B. L. Ingram, Department of Geology, Stanford University, Stanford, CA 94305, and Berkeley Center for Isotope Geochemistry, Department of Geology and Geophysics, University of California, Berkeley, CA 94720.
D. Sloan, Museum of Paleontology, University of California, Berkeley, CA 94720.

ing San Francisco Bay is from the northern catchment area by way of the Sacramento River and its tributaries. Only 15% of the water comes from the southeastern catchment area by way of the San Joaquin River and its tributaries. The other 5% of the freshwater comes from local sources such as the Napa and Petaluma rivers (Fig. 1) (*1*). Salinity in the estuary varies from marine conditions near the mouth of the bay to essentially riverine conditions near the delta (*1, 3*). The surfaces of equal salinity move toward the ocean as freshwater inflow increases and upstream as freshwater inflow decreases (*4*).

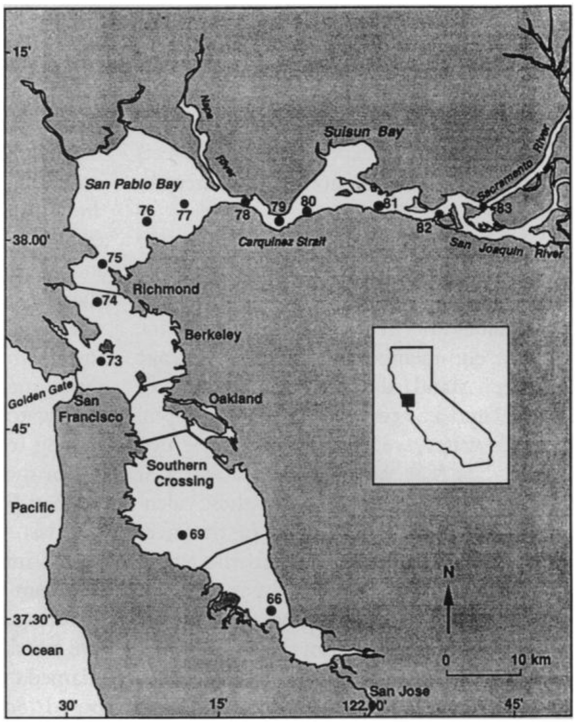

Fig. 2. Map of San Francisco Bay, showing localities where surface water was sampled and the Southern Crossing along which boreholes used in this study were taken.

Biogenic carbonate preserved in the estuarine sediments beneath the bay preserves information on salinity changes in the bay with time in the geologic past. The salinity record in the sediments is effectively averaged over at least several decades, because of bioturbation. Assuming an average sedimentation rate of 5.0 mm/year [the average Holocene sedimentation rate in central and south San Francisco Bay (*5*)] and a bioturbation depth of 10 cm, we expect that the salinity signal is an average over 20 years or more. Thus, salinity oscillations caused by diurnal tides and seasonal rainfall and snowmelt cycles are not resolvable in the sediments. During the last interglacial, relatively short-term salinity fluctuations (tens to hundreds of years) were superimposed on a 6000-year salinity cycle caused by the rise and fall of sea level related to changes in the volume of continental glacial ice.

To relate the $^{87}Sr/^{86}Sr$ variations measured in the fossil materials to salinity, we measured the Sr isotopic ratio and Sr concentration of seawater and river water entering the bay. Although the $^{87}Sr/^{86}Sr$ ratio in seawater has been increasing monotonically over the past 40 million years (*6, 7*), it has essentially remained the same for the past 400,000 years (*8*). The Sr concentration in seawater (7.9 ppm) has likewise probably not changed over this period (*9, 10*). In river water, the Sr isotopic composition reflects the $^{87}Sr/^{86}Sr$ ratio of the rocks being eroded in the catchment basin (*10–14*). We collected water from the major rivers and measured their Sr isotopic compositions and Sr and Rb concentrations (Fig. 1 and Table 1), using standard techniques (*15*).

The $^{87}Sr/^{86}Sr$ ratio of Sacramento River water near the mouth in the delta was 0.7062, and the $^{87}Sr/^{86}Sr$ ratio of water near the mouth of the San Joaquin River was 0.7073; these ratios are similar to those of the rocks in the drainage basin (*16, 17*). The Sr concentrations in the river waters also varied substantially. The highest Sr concentrations (118 to 176 ppb) were measured near the mouths of the San Joaquin and Sacramento rivers in the delta. These relatively high concentrations could be due to evaporation or anthropogenic input as the river crosses the San Joaquin Valley. However, these concentrations are within the range observed for rivers from other tectonically active areas (*10, 14*). We assume that the average Sr isotopic composition of river water entering the estuary during the last interglacial was not significantly different from our measured values, because the lithologies exposed in the drainage basin have not changed over at least the past few hundred thousand years. However, a southern shift in precipitation patterns over California, resulting in a larger portion of water entering the bay from the San Joaquin Riv-

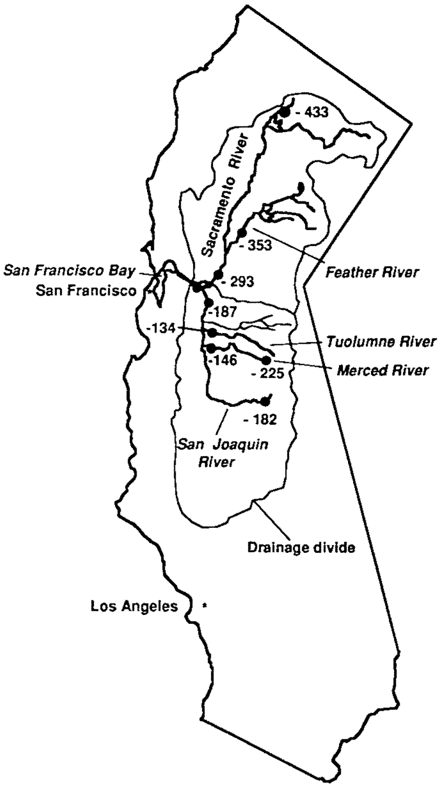

Fig. 1. Map of California showing drainage area and major rivers emptying into San Francisco Bay. Collection sites of river water samples and their measured $\Delta^{87}Sr$ values are plotted.

Table 1. Concentrations of Sr and Rb and Sr isotopic compositions of rivers draining into San Francisco Bay through the Sacramento–San Joaquin Delta. Locations of the samples plotted as $\Delta^{87}Sr$ values are shown in Fig. 1. River waters were collected July through September 1990.

Rb (ppb)	Sr (ppb)	$^{87}Sr/^{86}Sr \pm 2\sigma$	$\Delta^{87}Sr$
		Sacramento River	
2.2	56.9	0.704856 ± 30	−433
9.7	118.6	0.706257 ± 40	−293
		Feather River	
2.9	56.4	0.705663 ± 24	−353
		Merced River	
1.9	27.2	0.707407 ± 13	−178
3.4	49.4	0.707618 ± 16	−157
		0.707724 ± 8	−146
		0.706939 ± 8	−225
		Tuolumne River	
3.9	18.9	0.707851 ± 8	−134
		San Joaquin River	
	176.5	0.707315 ± 24	−187
1.4	10.9	0.707369 ± 18	−182

er, would increase the average riverine $^{87}Sr/^{86}Sr$ entering the bay. Also, the average Sr concentration in river water may have varied in the past. Although there may be ways of evaluating these effects, we have not yet done so; we do not expect that these effects will exert a large influence on our interpretation.

We calculated the relation between the Sr isotopic composition and salinity for the San Francisco Bay estuarine water and plotted $\Delta^{87}Sr$ values (*18*) in Fig. 3, A and B. For the seawater end-member, we used the average seawater standard $^{87}Sr/^{86}Sr$ value of 0.70919 and a Sr concentration of 7.9 ppm. For river water, we calculated the weighted average $^{87}Sr/^{86}Sr$ value of 0.7065 and a Sr concentration of 0.13 ppm. For these calculations, we assume that 80% of the river discharged into the bay is from the Sacramento River, and the remainder is from the San Joaquin River. Changing the proportion of river discharge from the San Joaquin River has only a small effect on the calculated curve (Fig. 3). An increase in the Sr concentration (due to increased evaporation or weathering rates in the past) would shift the mixing curve to the right (see Fig. 3).

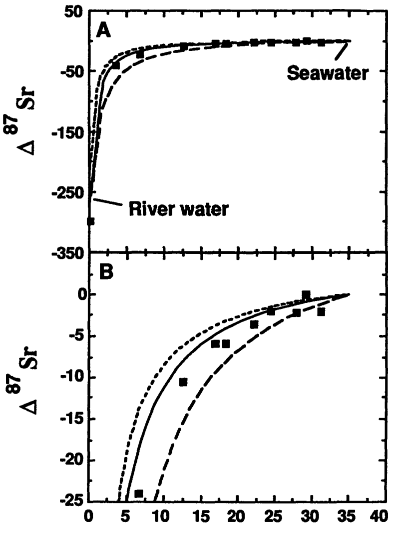

Fig. 3. (**A**) Calculated mixing curve between seawater (with a $\Delta^{87}Sr$ of 0 and a salinity of 35 per mil) and river water. The solid curve uses river water Sr concentration and $\Delta^{87}Sr$ as measured today (0.13 ppm and −280), as was used to calculate salinity from Sr isotopic data in this study. The short-dashed mixing curve uses a $\Delta^{87}Sr$ of −215 for river water, which would be the case if precipitation patterns changed and 50% of the water came from the San Joaquin River. The long-dashed mixing curve uses a river water Sr concentration of 0.26 (double that of today), which may be produced with increased evaporation or weathering rates. Measured Sr isotopic ratios and salinities (see Table 2) are also plotted. (**B**) Same as (A), with $\Delta^{87}Sr$ from 0 to −25.

In order to validate the relations among $^{87}Sr/^{86}Sr$ ratio, Sr concentration, and salinity in estuarine water, we analyzed surface water samples from the modern estuarine system (*19*), where the salinity ranges from 32 to 0.15 per mil (Fig. 2 and Table 2). The measured relation between Sr concentration and salinity is a mixing line between the two end-members (Fig. 4); this linear relation indicates that Sr behaves conservatively in the estuary (that is, Sr is not removed by or released from the sediments during the mixing of these water masses). The $^{87}Sr/^{86}Sr$ ratios measured on San Francisco Bay surface waters are very close to the calculated mixing relation (Fig. 3, A and B).

For the study of the salinity of the ancestral San Francisco Bay, which existed during the last interglacial maximum, well-preserved microfossil (foraminifera) were chosen from a suite of samples, previously processed for microfaunal analyses (*20*), from five boreholes drilled along a transect from Alameda to south San Francisco [the proposed "Southern Crossing" bridge site (Fig. 2)]. The estuarine unit, informally named the "Yerba Buena mud" (*20*), is the youngest pre-Holocene estuarine deposit in a sequence of estuarine-fluvial cycles during late Pleistocene glacioeustatic sea level fluctuations (Fig. 5) (*21, 22*). On the basis of its extent, stratigraphic relations, and amino acid racemization ages in mollusk shells from the upper part of the unit (*20–22*), the Yerba Buena mud is assumed to have been deposited during oxygen isotope substage 5e of the last interglacial (*23*). The unit has an average thickness of 31 m and is bracketed by alluvial and eolian sediments deposited during glacial periods of low sea level when the area now occupied by San Francisco Bay was a river valley (Fig. 5). On the basis of its average thickness and the depositional rates in south and central San Francisco Bay of 5 mm/year (*5*), we infer that deposition of the Yerba Buena mud spanned approximately 6000 years. The lateral extent of the Yerba Buena mud as found in borings drilled around the San Francisco Bay margin suggests that the ancestral San Francisco Bay was larger than the modern bay (*20, 24*), either because of higher sea level (which was 5 to 6 m higher during substage 5e) or because of minor subsidence. On the basis of ecological studies of foraminifers and sand-sized diatoms in the Yerba Buena mud (*20, 24, 25*), the depositional environments ranged from brackish marsh and shallow subtidal near the base to marine intertidal and subtidal at the top (*26*), which have been interpreted as representing increasing water depth and salinity upward in the section.

Table 2. Salinity, Sr concentration, and Sr isotopic composition of San Francisco Bay surface water samples (collection sites for the sample are plotted in Fig. 2 by sample number). Samples were collected on 11 March 1991.

Sample number	Salinity (per mil)	Sr (ppm)	$^{87}Sr/^{86}Sr \pm 2\sigma$	$\Delta^{87}Sr$
66	27.3	6.71	0.709160 ± 6	−2.9
69	29.5	6.57	0.709165 ± 6	−2.4
			0.709173 ± 7	−1.6
73	29.2	6.4	0.709189 ± 6	0.0
			0.709177 ± 6	−1.2
74	27.9	6.14	0.709167 ± 6	−2.2
			0.709163 ± 6	−2.6
75	24.4	5.62	0.709169 ± 6	−2.0
			0.709173 ± 6	−1.6
76	22.2	5.01	0.709153 ± 6	−3.6
			0.709160 ± 7	−2.9
77	18.4	4.52	0.709129 ± 6	−6.0
			0.709134 ± 7	−5.5
78	16.9	3.75	0.709130 ± 6	−5.9
			0.709130 ± 7	−5.9
79	12.6	2.6	0.709084 ± 6	−10.5
80	6.7	1.56	0.708949 ± 6	−24.0
81	3.6	1.04	0.708773 ± 6	−41.6
82	0.9	0.272	0.707885 ± 6	−130.4
83	0.15	0.104	0.706189 ± 6	−300.0
18	31.2	7.55	0.709168 ± 6	−2.1

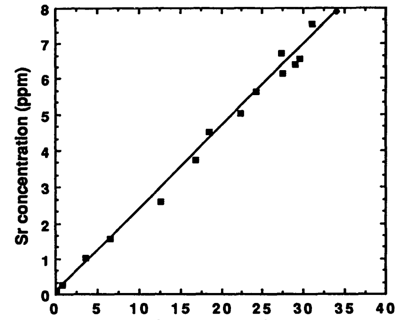

Fig. 4. Sr concentration versus salinity for San Francisco Bay surface waters.

We measured $^{87}Sr/^{86}Sr$ ratios and Sr concentrations from carbonate foraminifers from the Yerba Buena mud. The foraminifer shells were generally well preserved, and only those that showed no visible evidence of overgrowths or recrystallization were chosen for analysis. Samples weighing between 0.3 and 2.0 mg were cleaned ultrasonically in distilled water, dissolved, and analyzed for $^{87}Sr/^{86}Sr$ ratios (*27*). Given the young age of the samples and the impermeable nature of the mud in which they were encased, we expect that there was no postdepositional alteration of the $^{87}Sr/^{86}Sr$ ratio. On the basis of their lack of abrasion and high abundance in the sediments, we infer that the foraminifera grew in place and were not transported by currents. Because there is no detailed geochronology of the cores and the five cores used in this study were drilled

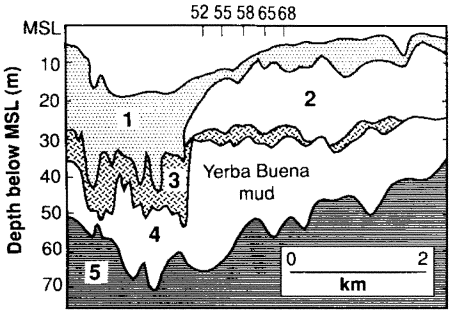

Fig. 5. Stratigraphic cross section constructed from boreholes drilled along the Southern Crossing, with depth below mean sea level (MSL). The section consists of five sedimentary units: 1, Holocene estuarine deposits; 2, Late Pleistocene to Holocene eolian deposits; 3, Late Pleistocene to Holocene alluvial deposits; 4, Pleistocene estuarine deposits (Yerba Buena mud); and 5, Pleistocene alluvial and estuarine deposits. The locations of the cores used for this study (52, 55, 58, 65, and 68) are shown at the top of the section.

within ~2 km of each other, samples were correlated by depth below mean sea level.

In general, a trend of increasing and then decreasing Δ^{87}Sr values with depth is seen in the data (Fig. 6A and Table 3). This general trend represents the large salinity variation in San Francisco Bay brought about by the rising and falling of sea level. We converted the Sr data to salinity (Fig. 6B) using the solid mixing curve in Fig. 3. The qualitative salinity ranges determined by the microfossil assemblages are in fairly good agreement with those determined by the Sr isotope compositions of fossil carbonate (Fig. 6B) (*26*). We also plotted the pre-1850 average salinity value (24 per mil) at Alameda, the closest salinity monitoring site to our core location sites. We estimated this value using the salinity-discharge relation given below and assuming a pre-1850 delta inflow rate of 1100 m^3/s (*28*), which is higher than the modern average discharge (~400 m^3/s) because of water diversion for irrigation and other purposes. Superimposed on the average longer term trend of rising and falling salinity were periods of higher and lower values, which appear to be of a cyclical nature.

These salinity data can be used to estimate delta outflow during the last interglacial, based on the relation between salinity and delta outflow determined for several sites in the bay from measurements made over the past 60 years (*4*). This relation for the Alameda monitoring site [modified from (*4*)], adjacent to our core locations along the Southern Crossing, is

$$S(Q) = S_0 e^{-0.25Q}$$

where $S(Q)$ is the salinity for a given river discharge Q, S_0 is the salinity at zero river discharge, and $e^{-0.25Q}$ is an exponential decay term relating salinity with delta outflow. Using this relation, we converted our salinity data to mean delta outflow (Fig. 6C). The pre-1850 average delta outflow was roughly the same as the mean delta outflow we calculated for the last interglacial (Fig. 6C). However, the salinity-delta outflow relation used is based on present-day sea level and bay geometry and therefore is not strictly correct for application to the late Pleistocene bay. More detailed modeling of the effect of changing bay volume from sea level fluctuation on the salinity-discharge relation will be needed to estimate correctly the paleodelta outflow relation. However, because the bay had a larger volume during the last interglacial, a greater delta outflow would have been required to produce the same salinity as in today's bay. Therefore, our estimates most likely underestimate the delta inflow during the last interglacial.

The delta outflow and salinity data show that there were times when the salinity and delta outflow were higher or lower than the mean. The aspect of this data set that needs further documentation, particularly for the Holocene record (10,000 years to the present), is that the salinity and delta outflow fluctuations appear to be cyclical with periods of hundreds of years. This implies a climatic forcing factor of a much shorter time scale than Milankovitch cycles, perhaps comparable to those seen in tree-ring width records in California (*29*), and has implications for water resource availability.

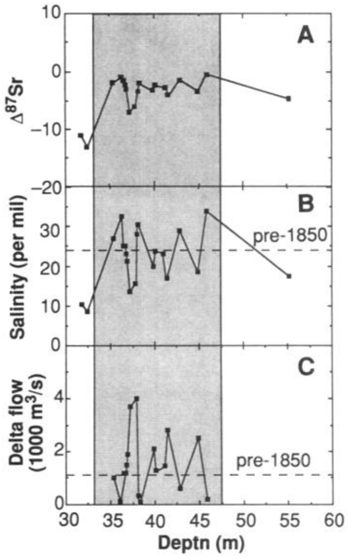

Fig. 6. (**A**) Δ^{87}Sr measured in foraminifera from the Yerba Buena mud plotted versus core depth. Sea level high stand for oxygen isotope substage 5e is shaded. (**B**) The salinity, determined from the Sr isotopic composition of the samples using the mixing curve in Fig. 4, plotted versus depth. The estimated pre-1850 average salinity at Alameda (24 per mil) is plotted for comparison. (**C**) Mean delta outflow, determined from the salinity-delta flow relation (*4*), versus depth for the sea level high stand. The pre-1850 mean delta flow is estimated to be almost twice today's delta flow (*28*).

Table 3. Sr isotopic compositions, biofacies, and depth in core of foraminifera samples from Yerba Buena mud cores. Each ^{87}Sr/^{86}Sr ratio is an average of two to three measurements.

Sample biofacies	Depth (m)	^{87}Sr/^{86}Sr ± 2σ	Δ^{87}Sr
55-14C	36.8	0.709165 ± 7	−2.4
52-15B	38.4	0.709190 ± 7	−0.1
52-17B	41.4	0.709140 ± 6	−4.9
55-16a/D	31.8	0.709077 ± 7	−11.2
55-16b/D	32.4	0.709057 ± 7	−13.2
55-19/C	35.4	0.709170 ± 8	−1.9
55-20b/B	36.9	0.709158 ± 5	−3.1
55-22z/B	39.7	0.709158 ± 7	−3.1
55-24a/B	42.7	0.709768 ± 8	−1.3
55-33/A	54.8	0.709148 ± 7	−4.1
58-18/B	36.5	0.709173 ± 7	−1.6
58-19/B	38.1	0.709172 ± 7	−1.7
58-21c/B	41.1	0.709162 ± 8	−2.7
65-20a/B	36.0	0.709180 ± 7	−0.9
65-20b/C	36.8	0.709118 ± 10	−7.1
65-22/C	39.9	0.709166 ± 7	−2.3
68-20a/C	35.4	0.709173 ± 5	−1.6
68-21/C	37.9	0.709125 ± 6	−6.4
68-24a/B	43.3	0.709155 ± 7	−3.4
68-24b/B	45.4	0.709184 ± 7	−0.5

We have demonstrated the applicability of using the Sr isotopic composition of biogenic precipitates in estuarine sediments as a proxy for salinity and delta outflow in the San Francisco Bay estuarine system over geologic time. This type of information can be used to establish delta outflow and salinity standards in San Francisco Bay and to assess precipitation variability for much of drought-prone California. This proxy salinity method may also be used in the assessment of natural freshwater inflow variability in other suitable estuarine and deltaic settings and may be used to detect large paleoclimatic events such as meltwater pulses, deglaciation, monsoonal variations, and floods.

REFERENCES AND NOTES

1. T. J. Conomos, R. E. Smith, D. H. Peterson, S. W. Hager, L. E. Schemel, in *San Francisco Bay: The Urbanized Estuary*, T. C. Conomos, Ed. (Pacific Division, AAAS, San Francisco, 1979), pp. 115–142.
2. D. R. Cayan and D. H. Peterson, in *Aspects of Climate Variability in the Pacific and the Western Americas*, D. H. Peterson, Ed. (Geophysical Monograph 55, American Geophysical Union, Washington, DC, 1989), pp. 375–397.
3. T. J. Conomos, in *San Francisco Bay: The Urbanized Estuary*, T. C. Conomos, Ed. (Pacific Division, AAAS, San Francisco, 1979), pp. 47–84.
4. D. H. Peterson *et al.*, in *Aspects of Climate Variability in the Pacific and the Western Americas*, D. H. Peterson, Ed. (Geophysical Monograph 55, American Geophysical Union, Washington, DC, 1989), pp. 419–442.
5. B. F. Atwater, C. W. Hedel, E. J. Helley, *U.S. Geol. Surv. Prof. Pap. 1014* (1977).

6. D. J. DePaolo and B. L. Ingram, *Science* **227**, 938 (1985).
7. J. Hess, M. L. Bender, J.-G. Schilling, *ibid.* **231**, 979 (1986).
8. R. C. Capo and D. J. DePaolo, *ibid.* **249**, 51 (1990).
9. H. D. Holland, *The Chemistry of the Atmosphere and Oceans* (Wiley, New York, 1978).
10. M. R. Palmer and J. M. Edmond, *Earth Planet. Sci. Lett.* **92**, 11 (1989).
11. G. W. Brass, *Geochim. Cosmochim. Acta* **40**, 721 (1976).
12. M. A. Wadleigh, J. Veizer, C. Brooks, *ibid.* **49**, 1727 (1985).
13. F. Albarede and A. Michard, *Chem. Geol.* **64**, 55 (1987).
14. S. J. Goldstein and S. B. Jacobsen, *ibid.*, p. 245.
15. River water was collected in 1-liter Teflon bottles and immediately acidified with 4 N nitric acid. The water (100 to 500 ml) was brought to dryness under a heat lamp, and K, Rb, and Sr concentrations were measured by isotopic dilution. For isotopic analyses, 100 ng of Sr in nitric acid, followed by 2 μl of a tantalum oxide–phosphoric acid slurry were evaporated onto a Re filament, which was then heated until red hot. The $^{87}\text{Sr}/^{86}\text{Sr}$ ratios were measured on a VG Sector 354 multicollector mass spectrometer in dynamic multicollection mode.
16. The San Joaquin River drains granitic and metamorphic rocks in the southern Sierra Nevada; these rocks have an average $^{87}\text{Sr}/^{86}\text{Sr}$ ratio of about 0.707 to 0.709. The Sacramento River drains the northern Sierra Nevadan granitic and metamorphic rocks and the young Cascade volcanic rocks, which have $^{87}\text{Sr}/^{86}\text{Sr}$ ratios of 0.704 to 0.707 (*17*).
17. R. W. Kistler and Z. E. Peterman, *Geol. Soc. Am. Bull.* **84**, 3489 (1973); U. Masi, J. R. O'Neil, R. W. Kistler, *Contrib. Mineral. Petrol.* **76**, 116 (1981).
18. We converted the $^{87}\text{Sr}/^{86}\text{Sr}$ ratios to $\Delta^{87}\text{Sr}$ values to allow interlaboratory comparison: $\Delta^{87}\text{Sr} = (^{87}\text{Sr}/^{86}\text{Sr}_{\text{sample}}) - (^{87}\text{Sr}/^{86}\text{Sr}_{\text{standard}}) \times 100{,}000$. Because the isotopic ratio can be measured to ±1 unit of $\Delta^{87}\text{Sr}$ (or 1 part in 10^5 of the $^{87}\text{Sr}/^{86}\text{Sr}$ ratio), the predicted relations (Fig. 3, A and B) show that the $^{87}\text{Sr}/^{86}\text{Sr}$ measurements are useful as a proxy for all salinities but are particularly sensitive for those less than about 25 per mil.
19. Surface water samples from San Francisco Bay were collected on 11 March 1991, in 0.5-liter Teflon bottles, by A. Van Geen, U.S. Geological Survey, Menlo Park, California. The samples were not acidified after collection, which may account for the slightly lower than expected Sr concentrations seen in many of the samples.
20. D. Sloan, thesis, University of California, Berkeley (1981).
21. B. F. Atwater *et al.*, in *San Francisco Bay: The Urbanized Estuary*, T. C. Conomos, Ed. (Pacific Division, AAAS, San Francisco, 1979), pp. 347–385.
22. ———, B. E. Ross, J. F. Wehmiller, *Quat. Res.* **16**, 181 (1981).
23. D. G. Martinson *et al.*, *ibid.* **27**, 1 (1987).
24. D. Sloan, *Geol. Soc. Am. Bull.*, in press.
25. ———, in *Quaternary Depositional Environments of the Pacific Coast*, M. E. Field *et al.*, Eds. (Society of Economic Paleontologists and Mineralogists, San Francisco, 1980), pp. 1–12.
26. The marsh environments (<10 m water depth) represented at the base of the Yerba Buena mud have low salinities (10 to 30 per mil), in which *Elphidium gunteri* and *Trochammina* are the dominant foraminifers (biofacies A). Samples from the middle of the unit represent subtidal environments with depths of 20 m or less and salinities from 15 to 35 per mil, with *Elphidium excavatum* and *Ammonia beccarii* as the dominant species (biofacies B). The upper samples in the boreholes represent marine intertidal to subtidal environments with salinity and temperature comparable to conditions along the coast today (33 to 35 per mil, water depths up to 50 m) in which *Elphidiella hannai* and *Buccella frigida* are common (biofacies C and D).
27. $^{87}\text{Sr}/^{86}\text{Sr}$ ratios were measured on 0.5- to 2-mg samples of carbonate foraminifera shells. The samples were cleaned ultrasonically with Nannopure water, dried, dissolved in weak acetic acid (to minimize contamination from noncarbonate phases such as clays), and then centrifuged. One aliquot of the sample was used to determine Sr and Rb concentrations by isotope dilution. Another aliquot was passed through an ion-exchange column to separate purified Sr. One hundred nanograms of purified Sr was used for isotopic analysis [see (*16*)].
28. F. H. Nichols, J. E. Cloern, S. N. Luoma, D. H. Peterson, *Science* **231**, 567 (1986).
29. H. C. Fritts, *Mon. Weather Rev.* **93**, 421 (1965); ———, G. R. Lofgren, G. A. Gordon, *Quat. Res.* **12**, 18 (1979).
30. We thank D. J. DePaolo for use of the laboratories at the Center for Isotope Geochemistry of the University of California, Berkeley, and the Lawrence Berkeley Laboratory, and for helpful discussion of the data and reviews of the manuscript. We also thank J. C. Ingle, W. B. N. Berry, E. Clifton, W. E. Dietrich, and D. H. Peterson who provided insightful discussions and comments.

19 July 1991; accepted 16 October 1991

Production of Isotopic Variability in Continental Basalts by Cryptic Crustal Contamination

ALLEN F. GLAZNER* AND G. LANG FARMER

Regional variations in the Nd, Sr, and Pb isotopic compositions of Neogene basalts from the western United States are commonly interpreted to originate in the subcontinental mantle. In southern California, isotopic variability is restricted to lavas that lack mantle-derived xenoliths; xenolith-bearing basalts have uniform isotopic compositions similar to those of ocean-island basalts (OIBs). Combined with available geochemical data, these observations suggest that isotopic variability at these volcanoes results from subtle crustal contamination, locally by mafic crust, of primitive OIB-like magma. Recognition of such cryptic contamination may help to reconcile local discrepancies between tectonic and isotopic views of the subcontinental mantle.

ISOTOPIC VARIATIONS IN BASALTS CAN yield information about the geodynamic history of the mantle. For example, variations in the Sr and Nd isotopic compositions of basalts have been used to infer the presence of old, isolated, lithospheric mantle beneath continents (*1–6*) and to track changes in mantle structure resulting from subduction and extension (*7, 8*). These conclusions are valid only if the basalts are unaffected by crustal contamination, but recent data (*9*) support Moyer and Esperança's (*10*) claim that isotopic variability can result from subtle crustal contamination that is not detectable by common geochemical screens.

In this study of Neogene basalts from the Mojave Desert of southern California we show that lavas bearing mantle xenoliths consistently have Nd and Sr isotopic compositions similar to those of modern-day ocean island basalts (OIBs), whereas xenolith-free basalts have a wider range of isotopic compositions that trend from OIB toward values expected for the continental lithosphere. This observation can be explained if xenolith-bearing magmas traversed the crust rapidly without interaction, whereas xenolith-free magmas stalled in the crust long enough for entrained xenoliths to be dropped or digested and for crustal interaction to occur.

Small-volume Neogene basalts occur throughout much of the Mojave Desert region (Fig. 1). These lavas range from alkali olivine basalts to hawaiites (*9, 11, 12*) and most have elemental characteristics that are traditionally invoked as evidence against significant silicic crustal contamination [high P_2O_5/K_2O ratios; high large-ion-lithophile, rare earth element, Sr, and Ni concentrations; and nepheline-normative compositions (*1, 2, 13, 14*)]. The lavas show a wide range of correlated Nd and Sr isotopic compositions (Table 1; Fig. 2), from values typical of asthenosphere-derived, OIBs ($\varepsilon_{\text{Nd}} = +6$ to $+9$ and $^{87}\text{Sr}/^{86}\text{Sr}$ ratios of 0.7025 to 0.7035) to values generally attributed to ancient lithospheric mantle underlying the North American craton [$\varepsilon_{\text{Nd}} = -3$ to $+6$ and $^{87}\text{Sr}/^{86}\text{Sr}$ ratios of 0.7035 to 0.7067 (*3, 6, 15, 16*)].

One interpretation of this data set is that low-ε_{Nd} basalts were derived from ancient lithospheric mantle and high-ε_{Nd} basalts from upwelling asthenospheric mantle. However, this interpretation fails to account for three aspects of the lavas: (i) lavas that carry mantle xenoliths (for example, peridotite) generally have OIB-like isotopic ratios, whereas lavas without mantle xenoliths scatter from OIB-like ratios to lower ε_{Nd} values and higher $^{87}\text{Sr}/^{86}\text{Sr}$ values (Fig. 2); (ii) the observation that high-ε_{Nd} and low-ε_{Nd} lavas are interleaved in both space and time (Ta-

---

A. F. Glazner, Department of Geology, University of North Carolina, Chapel Hill, NC 27599.
G. L. Farmer, Department of Geological Sciences and Cooperative Institute for Research in Environmental Science, University of Colorado, Boulder, CO 80309.

*To whom correspondence should be addressed.